Chapter 17
Internal Reflection of the Surface of a Plasmonic Substrate Covered by Active Nanoparticles

Eugene Bortchagovsky and Yurii Demydenko

17.1 Introduction

Surface plasmon polaritons (SPPs) are surface electromagnetic waves propagating along metal-dielectric [1, 2] or doped semiconductor-dielectric [2, 3] interfaces. Under phase-matching or resonance conditions, the energy of the exciting light wave is coupled to the collective oscillation of conducting electrons on the metal or semiconductor surface. There are a number of standard experimental methods for the realization of such an energy transfer [4, 5]. In the visible part of the spectrum, the Kretschmann configuration [5] based on a prism coupler with an active plasmonic film on its base is mainly used. Experimentally, the energy transferred at the excitation of a SPP wave is observed as a dip of a reflectance spectrum. As the excitation of the SPP wave has a resonant nature, the shape and the position of this minimum are highly sensitive to any changes in the refractive index at the surface of a plasmonic film. So, this configuration has been extensively applied to various chemical and biochemical sensing applications [6–9].

In the case when the surface of the plasmonic film is covered with a layer of active nanoparticles, SPP can act as a source of excitation of so-called localized plasmon polaritons (LPPs) [10–12] which, similar to conventional planar SPP in an extended system, are charge density oscillations confined within the nanoparticles. LPP is also resonant excitation, and the electromagnetic field of LPP near the surface of a nanoparticle may be strongly enhanced. Spectral properties of LPP depend on the material of nanoparticles, their structure, size, shape, and on the refractive index of local dielectric environment [12–17].

E. Bortchagovsky · Y. Demydenko (✉)
V. Lashkaryov Institute of Semiconductor Physics of National Academy of Sciences of Ukraine, Kyiv, Ukraine

O. Fesenko, L. Yatsenko (eds.), *Nanooptics, Nanophotonics, Nanostructures, and Their Applications*, Springer Proceedings in Physics 210,
https://doi.org/10.1007/978-3-319-91083-3_17

The interaction of LPPs excited on the nanoparticles with SPP waves leads to a modification of optical properties of SPPs which results, depending on the coupling of two excitations, in changing of the position of the minimum of reflectance (or the position of maximum of an absorption/extinction spectra of SPPs) or in the splitting of that minimum corresponding to the hybridization of two plasmonic modes. For the cases of high surface concentration of active nanoparticles on the surface of the plasmonic film, interactions between LPPs of individual nanoparticles lead to formation of a new collective long-range electromagnetic surface mode. In this case due to the interaction of this new mode with the SPP, we can definitely expect the mode hybridization and the occurrence of new minimum in reflectance (maximum in absorption/extinction) spectra of SPPs as well as to splitting of existed extremum [16–19].

For practical applications of plasmonic nanosystems, in particular in sensor applications, it is important to understand how one can govern their optical properties most efficiently by means of optimizing their structure and design [20–22]. In this connection the studying of the influence of parameters of the layer of active nanoparticles placed on the surface of an active plasmonic film on optical properties of such a system has both fundamental and practical interest.

In this paper we present general theoretical considerations of the influence of parameters of a layer of cylinder-like active nanoparticles placed on the surface of a plasmonic film on the reflectance spectrum measured in the Kretschmann configuration. Calculations of the optical properties of such a system are based on the Green function method [23, 24] taking into account of the local field effects in the system with uniformly distributed nanoparticles on the surface of the plasmonic film.

The paper is organized as follows: In Sect. 17.2 we give general remarks on the model and outline the geometry of the task. Section 17.3 deals with the common analytical method of the calculation of reflection coefficients for the chosen model. In Sect. 17.4 we apply the developed formalism for the numerical calculations of the reflection coefficient for the case of p-polarized excitation. These calculations are performed for the Kretschmann configuration assuming the uniform distributed cylindrical gold nanoparticles for the case when n-doped semiconductor F:SnO_2 is considered as the plasmonic substrate. The "mirror" case of exchanged materials of the nanoparticles and the substrate is considered as well. The shape and particle's concentration influence on the reflectance spectrum are scrutinized. Section 17.5 presents some conclusions for the results obtained in the presented work. In Appendix A we present the analytical calculation of the susceptibility of a single nanoparticle on a surface in the near-field approximation based on the effective susceptibility concept developed in [16, 17, 25–27]. In Appendix B the scheme of the calculation of the susceptibility of a nanoparticle layer within the Green function method is presented in brief [23, 24].

17.2 Problem Definition

Let us consider the Kretschmann scheme of the frustrated total internal reflection [5] with a glass prism covered by a thin film of a plasmonic material; on the surface of the film, a layer of active nanoparticles is placed, as it is depicted in Fig. 17.1. The incident radiation illuminates the plasmonic film in the Kretschmann scheme from the glass side at the angle of θ, and, for angles θ bigger than the Brewster angle, SPP wave can be excited at the interface of plasmonic film with environment.

The layer of active nanoparticles consists of identical cylindrical nanoparticles randomly distributed on the surface of the plasmonic film with the thickness h (Fig. 17.2). We will consider nanoparticles with diameter d and the height h_p, which are much less than the wavelength of light λ_0 (d, $h_p << \lambda_0$). Supposing that

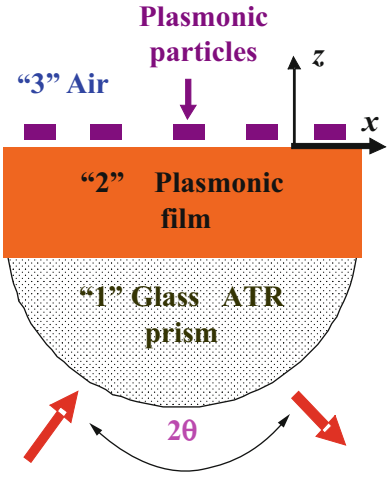

Fig. 17.1 Experimental scheme: Layer of cylindrical plasmonic nanoparticles is placed on a plasmonic film deposited on the base of a glass prism. The structure is illuminated in the Kretschmann configuration

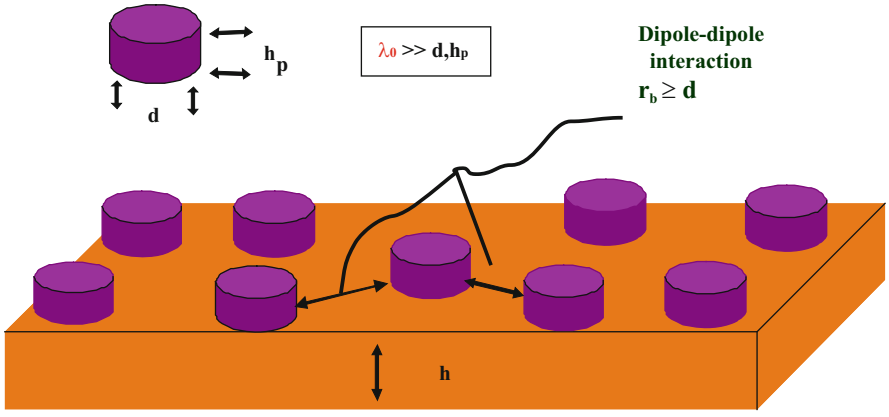

Fig. 17.2 Illustration of a particle layer placed on the surface of a plasmonic film. The particles are distributed randomly and uniformly with surface concentration *n*

the minimal distance between neighboring nanoparticles r_b is bigger than their diameter ($r_b \geq d$), one can treat interparticle interaction as dipole-dipole one [28].

The SPP wave interacts with localized plasmons of the active nanoparticles in the layer. As the properties of localized plasmons of nanoparticles strongly depend on the shape, size of nanoparticles, and the interaction between them, these properties depend on the concentration of particles on the surface. Thus, altering system parameters such as shape and particle concentration, one can change the optical properties of the whole system that results in modification of corresponding reflectance spectra.

17.3 Reflected Field

The reflected field $E^{(1)}(R,\omega)$ at the point **R** can be represented as superposition of two fields – the field reflected by the system without the layer of particles$E^{(01)}(R,\omega)$ and the field radiated by the particles

$$E^{(1)}(R,\omega) = E^{(01)}(R,\omega) - i\mu_0\omega\sum_{\upsilon=1}^{N}\int_{V_\upsilon} dR'_\upsilon \widetilde{G}^{(13)}\left(R,R'_\upsilon,\omega\right)j^{(3)}\left(R'_\upsilon,\omega\right), \quad (17.1)$$

with $\widetilde{G}^{(ab)}(R,R',\omega)$ the Green function (the photon propagator) describing field of frequency ω propagation from the source point $\mathbf{R}'$ in medium "a" to the observation point **R** in medium "b" for the system with two smooth interfaces [29]. The summation in Eq. (17.1) is over all positions υ which are occupied by the particles, $j^{(3)}\left(R'_\upsilon,\omega\right)$ is the induced current density within the υth particle, V_υ is the volume of the υth particle, and μ_0 is the vacuum permeability.

Supposing of a local relation between the current density $j^{(3)}\left(R'_\upsilon,\omega\right)$ and the local field $E^{(3)}\left(R'_\upsilon,\omega\right)$ at the point R'_υ, one can write

$$j^{(3)}\left(R'_\upsilon,\omega\right) = -i\omega\varepsilon_0\widetilde{\chi}(\omega)E^{(3)}\left(R'_\upsilon,\omega\right), \quad (17.2)$$

with $\widetilde{\chi}(\omega) = \left(\widetilde{\varepsilon}(\omega) - \widetilde{U}\right)/4\pi$, where $\widetilde{\chi}(\omega)$ and $\widetilde{\varepsilon}(\omega)$ are the linear response to the local field $E^{(3)}\left(R'_\upsilon,\omega\right)$ and the dielectric function of the material of particles, ε_0 is the vacuum permittivity, and $\widetilde{U}$ is the unit tensor.

Inserting this expression for $j^{(3)}\left(R'_\upsilon,\omega\right)$ into Eq. (17.1), one can write

$$E^{(1)}(R,\omega) = E^{(01)}(R,\omega) - k_0^2\sum_{\upsilon=1}^{N}\int_{V_\upsilon} dR'_\upsilon \widetilde{G}^{(13)}\left(R,R'_\upsilon,\omega\right)\widetilde{\chi}(\omega)E^{(3)}\left(R'_\upsilon,\omega\right), \quad (17.3)$$

where $k_0^2 = \omega/c$ and c is the light velocity. Considering each particle as the point-like dipole located at its center of mass with the polarizability of the cylindrical particle (the so-called quasi-point-like approximation [24–26]), the second term of Eq. (17.3) can be rewritten in the form

$$\sum_{\upsilon=1}^{N} \int_{V_\upsilon} dR'_\upsilon \widetilde{G}^{(13)}\left(R, R'_\upsilon, \omega\right)\widetilde{\chi}(\omega)E^{(3)}\left(R'_\upsilon, \omega\right)$$

$$\approx V \sum_{\upsilon=1}^{N} \widetilde{G}^{(13)}\left(r - r'_\upsilon, z, z_c, \omega\right)\widetilde{\chi}^{(S)}(\omega)E^{(3)}\left(r'_\upsilon, z_c, \omega\right), \tag{17.4}$$

where vectors r'_υ define the positions of the particles in the z_c-plane and z_c denotes the z-coordinate of the center of mass of a particle. The tensor, $\widetilde{\chi}^{(s)}(\omega)$, introduced in Eq. (17.4) determines the linear response of a cylindrical particle on the surface of a substrate to the local field acting inside the particle volume V (the dimensionless polarizability). The implicit expression of $\widetilde{\chi}^{(s)}(\omega)$is given in Appendix A.

Taking into account that the considered system is homogeneous in the XOY plane, it is possible to perform the Fourier transformation of Eq. (17.4) in the plane and to average the obtained result with the function of the homogeneous distribution [25–27]. Then Eq. (17.3) for the reflected field $E^{(1)}(k, z, \omega)$ at the observation point z is written in the **k**-z representation as

$$E^{(1)}(k, z, \omega) = E^{(01)}(k, z, \omega) - \rho\widetilde{G}^{(13)}(k, z, z_c, \omega)\widetilde{\chi}^{(S)}(\omega)E^{(3)}(k, z_c, \omega), \tag{17.5}$$

with $\rho = Vk_0^2 n$, where n is a concentration of nanoparticles on the surface of the plasmonic film. $E^{(01)}(k, z, \omega)$ is the field reflected in Kretschmann configuration from the structure without the layer of particles

$$E^{(10)}(k, z', \omega) = -i\mu_0\omega \int_{l_0} dz'' \widetilde{G}_I^{(11)}(k, z', z'', \omega) j^{1ext}(k, z'', \omega), \tag{17.6}$$

where $\widetilde{G}_I^{(11)}$ is the indirect part of the Green's function [29] and $j^{1ext}(k, z'', \omega)$ is the current density of a source of the external to the system field.

Using connection between local field $E^{(3)}(k, z_c, \omega)$ and the external field acting on a nanoparticle in the layer $E^{(30)}(k, z_c, \omega)$, which is given by Eq. (17.B6), Eq. (17.5) takes the form

$$E^{(1)}(k, z, \omega) = E^{(01)}(k, z, \omega)$$
$$- \rho\widetilde{G}^{(13)}(k, z, z_c, \omega)\widetilde{\chi}^{(S)}(\omega)\widetilde{\Omega}(k, z_c, z_c, \omega)E^{(30)}(k, z_c, \omega) \tag{17.7}$$

with

$$E^{(30)}(k, z_c, \omega) = -i\mu_0\omega \int_{l_0} dz'' \widetilde{G}^{(31)}(k, z_c, z''\omega) j^{1ext}(k, z'', \omega). \tag{17.8}$$

Supposing that the source of the external electric field is a point dipole located at z_0, we can write

$$j^{1ext}(k,z'',\omega) = j^{1ext}(k,\omega)\delta(z''-z_0). \tag{17.9}$$

Substituting Eq. (17.9) into Eq. ((17.7), we receive

$$E^{(1)}(k,z,\omega) = -i\mu_0\omega\Big(\widetilde{G}_I^{(11)}(k,z,z_0,\omega) - \rho\widetilde{G}^{(13)}(k,z,z_c,\omega)\widetilde{\chi}(\omega)\widetilde{\Omega}\big(k,z_c,z_c,\omega\big)\widetilde{G}^{(31)}\big(k,z_c,z_0,\omega\big)\Big)j^{1ext}(k,\omega). \tag{17.10}$$

Taking into account the explicit expressions of the Green function [29], Eq. (17.10) may be rewritten in the form

$$E^{(1)}(k,z,\omega) = -i\mu_0\omega e^{æ_1 z}\Big(\widetilde{G}_I^{(11)}(k,\omega) - \rho\widetilde{T}^{(11)}\big(k,\omega\big)\Big)j^{(1ext)}(k,z_0,\omega), \tag{17.11}$$

where the next designations are introduced

$$\widetilde{T}^{(11)}(k,\omega) = \widetilde{G}^{(13)}(k,\omega)\widetilde{\chi}(\omega)\widetilde{\Omega}(k,z_c,z_c,\omega)\widetilde{G}^{(31)}(k,\omega)\exp(-2æ_3 z_c), \tag{17.12}$$

$$j^{(1ext)}(k,z_0,\omega) = j^{(1ext)}(k,\omega)\exp(-æ_1|z_0|), \tag{17.13}$$

$$æ_u = \sqrt{|k|^2 - \varepsilon_u k_0^2}, \quad (u=1,2,3) \tag{17.14}$$

with ε_u denoting dielectric constants of media constituting the system.

To calculate the reflectance of the system, the expression for the field illuminating the system $\mathbf{E}^{(1ext)}$ is necessary, which can be obtained via the direct part of the Green's function, $\widetilde{G}_D^{(11)}$ [29]

$$E^{(1ext)}(k,z,\omega) = -i\mu_0\omega e^{-æ_1 z}\widetilde{G}_D^{(11)}(k,\omega)j^{1ext}(k,z_0,\omega). \tag{17.15}$$

Dividing the field on s- and p-polarized components, we can calculate corresponding reflectivities R_s and R_p from Eqs. (17.11) and (17.15):

$$R_s(k,\omega) = \left|G_{Iyy}^{(11)}(k,\omega) - \rho T_{yy}^{(11)}\big(k,\omega\big)\right|^2 \Big/ \left|G_{Dyy}^{(11)}(k,\omega)\right|^2, \tag{17.16}$$

$$\begin{aligned} &R_p(k,\omega) \\ &= \left(\begin{array}{l} \left|\left(G_{Ixx}^{(11)}(k,\omega) - \rho T_{xx}^{(11)}\big(k,\omega\big)\right)\cos\theta + \left(G_{Ixz}^{(11)}(k,\omega) - \rho T_{xz}^{(11)}\big(k,\omega\big)\right)\sin\theta\right|^2 \\ +\left|\left(G_{Izx}^{(11)}(k,\omega) - \rho T_{zx}^{(11)}\big(k,\omega\big)\right)\cos\theta + \left(G_{Izz}^{(11)}(k,\omega) - \rho T_{zz}^{(11)}\big(k,\omega\big)\right)\sin\theta\right|^2 \end{array}\right) \\ &\Big/\left(\left|G_{Dxx}^{(11)}(k,\omega)\cos\theta + G_{Dxz}^{(11)}\big(k,\omega\big)\sin\theta\right|^2 + \left|G_{Dzx}^{(11)}(k,\omega)\cos\theta + G_{Dzz}^{(11)}\big(k,\omega\big)\sin\theta\right|^2\right). \end{aligned} \tag{17.17}$$

Eqs. (17.16) and (17.17) were written under assumption that $Re\varepsilon_1 = 0$ (a nonabsorbing glass prism).

17.4 Numerical Calculation of Reflectance Spectra and Discussion

We will consider two "mirror" cases with respect to active materials of nanoparticles and the plasmonic film. In the first case, metallic cylindrical particles are placed on the surface of a thin film of a n-doped semiconductor transparent in the visible, as it is shown in Figs.17.1 and 17.2 and the second case when the materials of the particles and the substrate are replaced by each other.

Let us suppose that optical properties of the considered system can be described rather adequately taking the dielectric functions of a metal in Drude form:

$$\widetilde{\varepsilon}(\omega) = \left[\varepsilon_{1\infty} - \omega_p^2/\left(\omega^2 + i\omega\gamma_p\right)\right]\widetilde{U}, \tag{17.18}$$

where $\varepsilon_{1\infty}$ is the optical high-frequency dielectric constant of a metal and ω_p and γ_p are the plasma frequency and the rate constant for the metal, respectively. We shall take the dielectric function of a n-doped semiconductor in the form

$$\widetilde{\varepsilon}(\omega) = \varepsilon_{2\infty}\left[1 + \left(\omega_{LO}^2 - \omega_{TO}^2\right)/\left(\omega_{TO}^2 - \omega^2 - i\omega\gamma_{ph}\right) - \widetilde{\omega}_e^2/\left(\omega^2 + i\omega\gamma_e\right)\right]\widetilde{U}, \tag{17.19}$$

with $\varepsilon_{2\infty}$ denoting the optical high-frequency dielectric constant of a semiconductor; ω_{LO}, ω_{TO}, and γ_{ph} are the transverse and longitudinal frequency of the optical phonons and the phonon damping constant, respectively; and $\widetilde{\omega}_e = \omega_e/\sqrt{\varepsilon_{2\infty}}$, ω_e, and γ_e are the plasma frequency and the damping rate constant of free electrons for the doped semiconductor, respectively. The following effective parameters were taken for the dielectric function of metal (gold) [30]: $\varepsilon_{1\infty} = 9{,}84$, $\omega_p = 1{,}38{\cdot}10^{16}\ s^{-1}$, and $\gamma_p = 1{,}09{\cdot}10^{14}\ s^{-1}$. Fluorinated tin oxide (F:SnO_2) is considered as a n-doped semiconductor with the following effective parameters [31]: $\varepsilon_{2\infty} = 3{,}19$, $\omega_{LO} = 9{,}03{\cdot}10^{15}\ s^{-1}$, $\omega_{TO} = 7{,}99{\cdot}10^{15}\ s^{-1}$, $\omega_e = 2{,}24{\cdot}10^{15}\ s^{-1}$, $\gamma_{ph} = 1{,}94{\cdot}10^{14}\ s^{-1}$, and $\gamma_e = 2{,}54{\cdot}10^{14}\ s^{-1}$.

We will consider the case when p-polarized radiation excites the system coming from the medium "1" at the angle of incidence θ=60^0 in the (XOZ) plane (Fig. 17.1). The BK7 glass prism with the refraction coefficient $n_{pr} = 1{,}47$ is considered as the medium "1", and the wave vector of the incident radiation is $k = \left(k_0 n_{pr}\sin\theta e_x, 0\right)$. The thickness of the active layer $h = 50$ nm is chosen the same for both considered cases.

Sizes of cylindrical gold nanoparticles were taken as $h_p = 25$ nm and $d = 100$ nm, and their dielectric function was obtained by Eq. (17.18). Then, considering F:SnO2 as the active film with dielectric function defined by Eq. (17.19), numerical

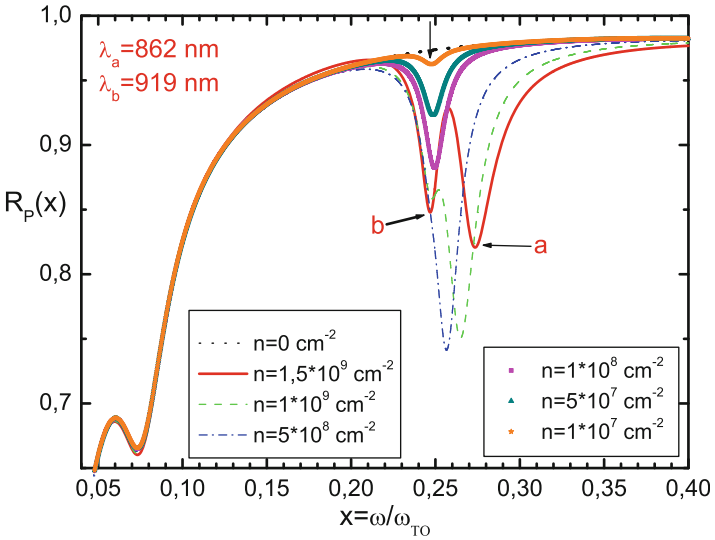

Fig. 17.3 Influence of the particle concentration n on the reflectance spectra. The spectra calculated for the case with F:SnO_2 as a substrate for gold particles. The angle of incidence $\theta = 60^0$

calculations of an influence of the surface concentration n on the reflection spectrum of the system in the Kretschmann geometry were performed using Eq. (17.17). The results are presented in Fig. 17.3.

As it is seen from Fig. 17.3, the reflection spectra for selected parameters remarkably depend on the particle concentration. Without gold particles on the surface of F:SnO_2, there is only one dip in the reflectance spectra around normalized frequency $x = 0{,}07$ connected with the excitation of the plasmon of a subsystem of conducting electrons. Deposition of gold particles results in the arising of a new dip close to $x = 0{,}25$ corresponding to the excitation of out of plane localized plasmons. The spectral position of this localized plasmon for one separated nanoparticle on the surface of F:SnO_2 film is $x = 0{,}248$, which is shown in figures by arrow. At small particle concentration of about $n \leq 10^7$ cm^{-2}, this dip is not pronounced but further rises with the increase of the number of particles. This behavior is obvious as the absorbed energy should correlate with the number of absorbers. However, the depth of the minimum rises not linear with the number of particles became slower at bigger concentrations. Along with the increase of the depth of that minimum, its blue shift is observed (spectral positions of sequential minima are given in Fig. 17.3 and shown in Fig. 17.4). It is the exhibition of interparticle interactions that results in the creation of common mode of the ensemble of degenerated localized plasmons of individual particles. The blue shift also indicates that we observe out of plane plasmonic resonance of nanoparticles [32]. The blue shift becomes more pronounced for concentrations of particles more than $1{\cdot}10^8$ cm^{-2}.

However, this behavior of the minimum changes remarkably after the concentration exceeds about $5{\cdot}10^8$ cm^{-2}. One minimum splits demonstrating at $x \approx 0{,}245$

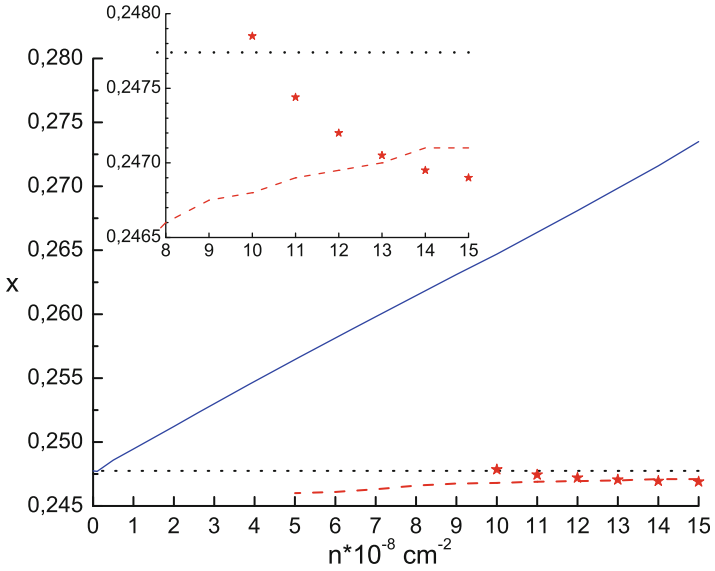

Fig. 17.4 Position of minima in reflectivity spectra versus the concentration of nanoparticles on the surface. Dashed line gives the position of the resonance of one separated particle as blue and red ones of two blue and red shifted minima noticed in Fig. 17.3 by a and b correspondingly. The insert demonstrates the position of red shifted minimum in more details. The line represents the position defined from the second derivative as stars by visually visible minimum positions

small minimum as the deep one moves to the blue side to about $x = 0{,}26$. Further increase of the concentration makes both minima equally pronounced with smaller but comparable depths indicated in Fig. 17.3 by letters "a" and "b." The spectral position of the second dip gets about $x \approx 0{,}275$ at the highest concentration $1{,}5 \cdot 10^9$ cm^{-2} what is about the limit to which we can restrict ourself by dipole-dipole interactions. This behavior demonstrates the transfer from weak coupling of SPP with collective mode of nanoparticles to strong one with their hybridization and splitting. It happens when the energy of coupling exceeds the damping [33] and modes can exchange energy of excitation many times before decay.

Fig. 17.4 exhibits the normalized spectral position of minima of reflectivity spectra versus the surface concentration of nanoparticles on the surface. Two branches, which correspond to two minima shown in Fig. 17.3, are visible. It is interesting that the behavior of the blue shifted minimum noticed in Fig. 17.3 by "a" is practically linear with the concentration. The second minimum becomes noticeable only at concentrations higher than $5 \cdot 10^8$ cm^{-2} and visually recognizable after $1 \cdot 10^9$ cm^{-2}. The positions of that red shifted minimum were defined either from the second derivative revealing flex points of the curve what is shown by solid line or from the visually recognizable minima position (first derivative) at higher concentrations what is shown by stars. The difference behavior of stars can be explained by the influence of not well-separated blue shifted minimum and the exhibition of the red shifted minimum as a shoulder on the dip of the blue shifted minimum. It gives

visually shifted minimum position to the direction of the main minimum (in our case to blue side) according to the real one. It is obvious that the flex point should be closer to the minimum position just when it is very shallow and not revealed by the first derivative. Finite numerical precision explains not smooth behavior of the flex point.

Despite shown dependences are not dispersion curves, demonstrated behavior proves that we have different coupling conditions for surface and localized resonances at different concentration of deposited nanoparticles in the system gold nanoparticles – n-doped semiconductor F:SnO_2 and transfer between these two regimes. To demonstrate this transfer more pronouncedly, reflectivity of our system is shown in more details in Fig. 17.5 for three ranges of the particle concentration: small up to $1{\cdot}10^8$ cm^{-2}, intermediate from $1{\cdot}10^8$ cm^{-2} to $5{\cdot}10^8$ cm^{-2}, and high up to $1{,}5{\cdot}10^9$ cm^{-2}.

Panel 4a shows sequential increasing of the depth of the absorption dip with rather small blue shift, as the average distances between particles in our system at the concentration $1{\cdot}10^8$ cm^{-2} are still rather large of about 1 μm remarkably exceeding

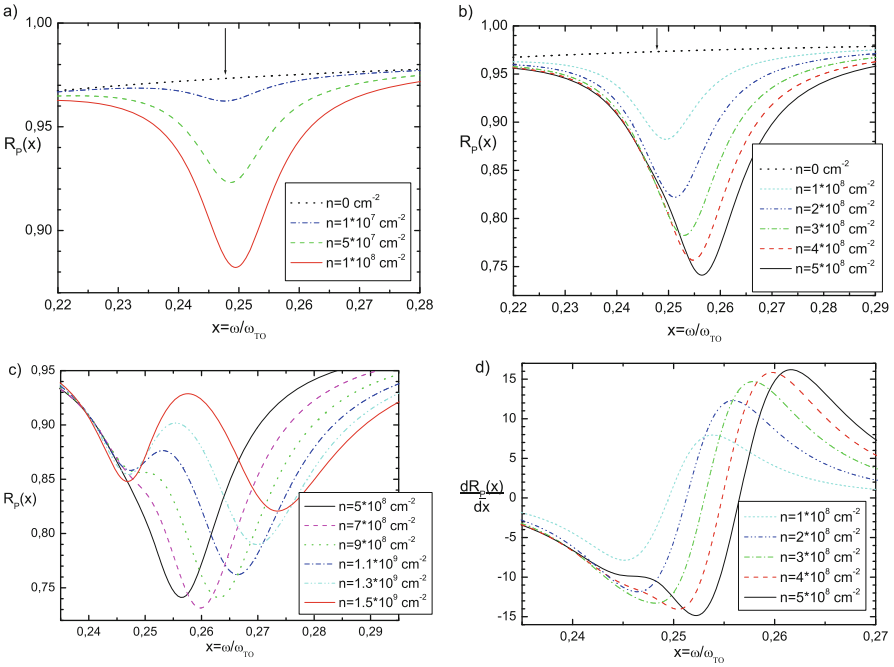

Fig. 17.5 Detailed presentation of the reflectivity from Fig. 17.3 for different ranges of concentrations: (**a**) small ones up to $1{\cdot}10^8$ cm^{-2}, (**b**) intermediate ones for the range $1 \div 5{\cdot}10^8$ cm^{-2}, (**c**) high ones over $5{\cdot}10^8$ cm^{-2}, and (**d**) the first derivatives of curves from the panel b

the lateral size of the particle. Panel 4b exhibits the range of intermediate concentrations of $1 \div 5 \cdot 10^8$ cm^{-2}. For this range pronounced blue shift is visible up to about x ≈ 0,255 what is far from the position of the resonance of the only particle indicated by arrow. Panel 4c exhibits the case of higher concentrations when the splitting of minima is clearly visible. It may be seen that the position of the resonance at x ≈ 0,245 is practically nonshifted from the resonance of one separated particle. So this resonance corresponds to the localized-like branch of two hybridized modes.

It is necessary to note that careful consideration of the reflectance curve for the concentration of $5 \cdot 10^8$ cm^{-2} reveals its slight asymmetry. To clarify it, first derivatives of curves from panel 4b are shown in panel 4d. It is clearly seen that already at the concentration of $5 \cdot 10^8$ cm^{-2} and less pronounced at $4 \cdot 10^8$ cm^{-2}, there is the trace of the second minimum corresponding to the localized-like mode. It means that already at the distance between edges of particles exceeding their size in $1.5 \div 2$ times, there is the creation of the common mode of the layer and their hybridization with the surface plasmon of the substrate resulting in the splitting of two modes. The hybridization of modes at smaller concentration is probably absent. At least even the second derivative does not demonstrate any additional features beside of the one resonance for the concentration of $3 \cdot 10^8$ cm^{-2}.

So we suppose that presented three diapasons of the particle concentration correspond to three different coupling regimes for surface and localized plasmons in the considered system. At small concentrations of nanoparticles when interparticle interactions are practically unobservable, there is weak coupling of modes. Rising the concentration of deposited nanoparticles, we come to the case of noticeable interparticle interactions resulting in the shift of the common resonance of the layer of nanoparticles, but still intermediate coupling of surface and localized modes when the strength of the coupling is comparable with the mode dumping [33] and splitting is not yet pronounced. Only the trace of the splitting is visible in this case as the shoulders of the reflectivity spectrum. The third regime of strong coupling with pronounced Rabi splitting is realized at high particle concentration.

As it is well known [34, 35], the positions of minima of the reflectance spectrum at the excitation of SPPs are determined by the positions of zeroes of the pole part of the susceptibility of the considered system. These zeroes define points on the plane (θ,ω) where SPPs can be excited under given parameters of the system. The number of these points determines curves, which are dispersion characteristics of excited SPPs. In the case considered in this work, the appropriate zero points can be obtained from the equation

$$\mathrm{Re}\left\{\det\left[\left(\widetilde{\Omega}\left(k, z_c, z_c, \omega\right)\right)^{-1}\right]\right\} = 0, \quad \left(k = k_0 n_{pr} \sin\theta\right). \tag{17.20}$$

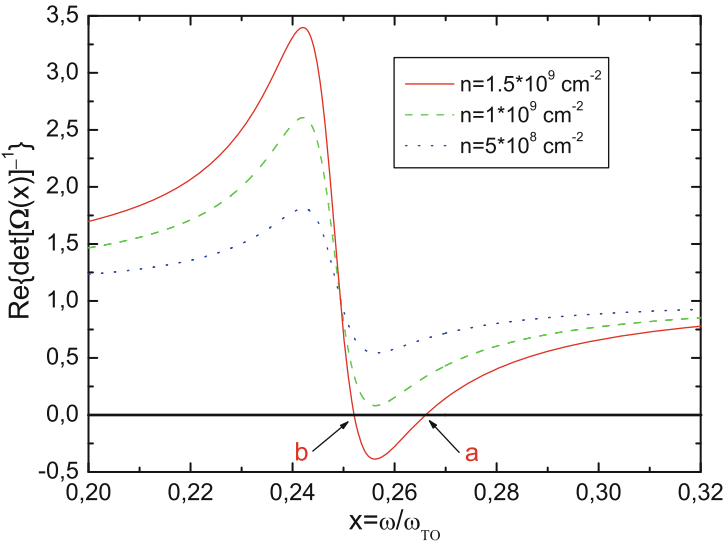

Fig. 17.6 The illustration of the appearance of zeroes of the pole part of $\widetilde{\Omega}(k, z_c, z_c, \omega)$when the surface nanoparticle concentration, n, increases

Let us consider the plot of $\mathrm{Re}\left\{\det\left[\left(\widetilde{\Omega}(k, z_c, z_c, \omega)\right)^{-1}\right]\right\}$ as the function of the normalized frequency $x = \omega / \omega_{TO}$ for the case of high concentration of nanoparticles with parameters used in previous calculations. These curves are shown in Fig. 17.6 for different concentrations of nanoparticles.

As it is seen from Fig. 17.6, for the nanoparticle concentrations for which $n \geq 1{\cdot}10^9$ cm^{-2}, one can say that requirement of the excitation of SPP waves in the considered system is satisfied. The discrepancy of this value with the value $n \geq 5{\cdot}10^8$ cm^{-2}, obtained in the analysis of reflectance spectra, may be explained by damping. Only at $n \geq 1{\cdot}10^9$ cm^{-2}, two minima are well seen, before the red one is seen only as the shoulder on the curve. The account of damping would correspond to the spreading of linear curves in Fig. 17.6 to stripes, so even at smaller concentrations, there would be touching of zero line corresponding to the excitation of SPP in the system.

As it was already mentioned in the introduction [12–17], optical properties of LPP strongly depend on the shape of the nanoparticle. Thus, we can expect effective control of the optical properties and the reflectance spectra of the system modifying the shape of deposited nanoparticles. Let us fix the particle concentration at $n = 1{,}5{\cdot}10^9$ cm^{-2} and the value of the particle volume at $V = 1{,}96{\cdot}10^{-22}$ m^3 (the value of the volume corresponds to $h_p = 25$ nm and $d = 100$ nm; these geometrical parameters will be used as initial ones) and study numerically the influence of the change of the particle shape on the reflectance spectrum using Eq. (17.17) with the

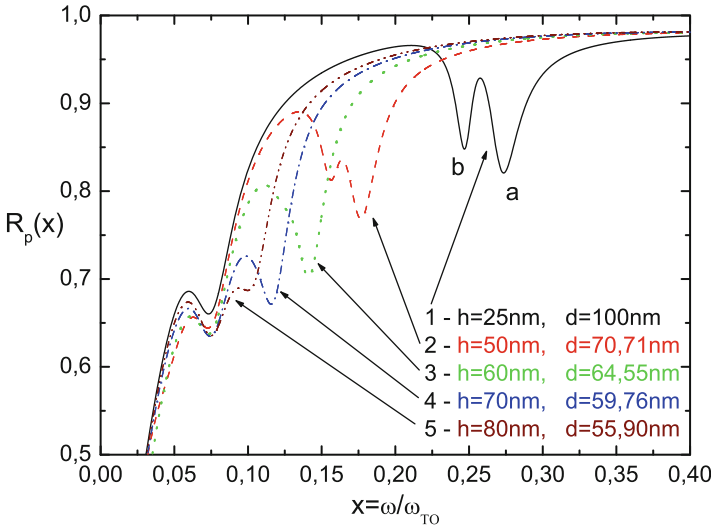

Fig. 17.7 The influence of the modification of the particle shape on the reflectance spectrum for the case of high particle concentration. For all curves the particle volume V is taken constant

same other parameters of the system as it was used in previous calculations. The result of these calculations is presented in Fig. 17.7.

As it is seen from Fig. 17.7, the change of the particle form from the disk-like to pillar-like one leads to quick disappearance of the "red" (b) localized-like mode. This happens along with rapid displacement of the remaining "blue" (a) toward low frequencies that results in the disappearance of this minimum at the frequency of SPP mode of the F:SnO_2 substrate at given angle of incidence $\theta = 60^0$. The local field interactions of localized plasmons of nanoparticles with surface plasmonic excitation of conducting electrons on the F:SnO2 substrate lead to slight improvement of SPP generation condition exhibited by a bit dipper minimum at $x = 0{,}07$.

Let us exchange the materials of deposited nanoparticles and the active film assuming semiconducting particles on gold and using Eq. (17.17) consider the influence of particle concentration on the reflectance spectrum of such a modified system in the same way as it was done for the previous system presented in Fig. 17.3. The incident angle of external radiation is now $\theta = 44^0$, as for angles of incidence bigger than 50^0, the minimum in reflectivity spectra is not pronounced. The height and diameter of nanoparticles are the same as for Fig. 17.3. At these conditions the well-known SPP is generated on the surface of gold layer. The field of SPP interacts with the disk-like nanoparticles of F:SnO_2 that leads to worsening of the generation condition of the SPP wave at high concentrations, and, as the result of the interaction, the minimum of SPP becomes shallower and a bit shifted than for the clean surface of a gold film. The result of calculations is shown in Fig. 17.8. So, no

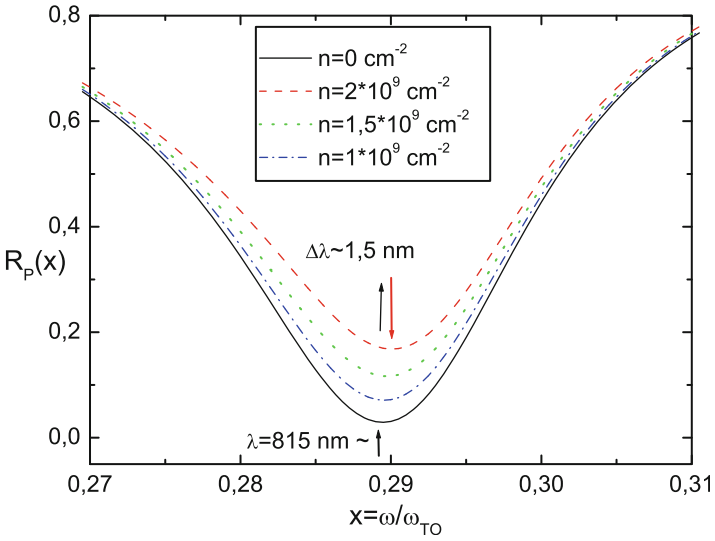

Fig. 17.8 The influence of particle concentration *n* on the reflectance spectra of "reversed" structure with semiconducting particles on the gold film

distinctive influence on the reflectance spectrum is found but the fact that loading of active semiconducting particles of F:SnO_2 gives slight blue shift of the plasmonic resonance in contrast to deposition of any passive material on the gold surface.

17.5 Conclusion

Within the frame of the Green functions method with the use of the concept of effective susceptibility the approach for the calculation of reflectance spectra of the layer of possessing LP cylindrical nanoparticles situated on the surface of a plasmonic film was developed. The modeling was performed for the system of gold disks on the surface of the n-doped semiconductor F:SnO_2 for the illumination of the system in the Kretschmann configuration with the excitation of SPP. The dependences of the reflectivity on the particle concentration and on their shape were investigated. Obtained results clearly demonstrate the possibility of effective control of optical properties of the system and its reflectance spectrum changing parameters of the layer of particles. The spectral position of resonances of such a system can be tuned by changing the particle shape.

Investigation of the concentration dependence of the optical properties of the considered system reveals the existence of regions of weak and strong coupling of surface and localized modes and clear transition from one to the other regime. At higher concentration of deposited nanoparticles, damping of the common mode of nanoparticle layer, which is created from degenerated localized resonance by

interparticle interactions, drops, and we obtain the strong coupling regime with the hybridization of modes and Rabi splitting. This transition between two regimes was analyzed in detail.

The system considered in this study can be used as active element of sensors.

Appendices

Appendix A

Susceptibility of a Nanoparticle on the Surface in the Near-Field Approximation

Let us consider a cylindrical nanoparticle placed on the surface of an isotropic active plasmonic substrate (metal or n-doped semiconductor) with the dielectric constant $\varepsilon_2(\omega)$ illuminated by long-range electrical field $\mathbf{E}^{(0)}(\mathbf{R},\omega)$ as it is illustrated in Fig. 17.2. As linear dimension of the particle is supposed less than the wavelength, all electrodynamic interactions between the particle and the substrate as well as with a surrounding medium can be taken into account by using the Green function in near-field approximation [16, 17]. Then the local field $\mathbf{E}(\mathbf{R},\omega)$ at any point $\mathbf{R}$ in the system can be calculated by the equation

$$E(R,\omega) = E^{(0)}(R,\omega) - i\omega\mu_0 \lim_{\delta\to 0} \int\limits_{V-V_\delta} dR' \widetilde{G}^{NF}\left(R,R',\omega\right) j\left(R',\omega\right) - \frac{1}{i\omega\varepsilon_0}\widetilde{L} j(R,\omega), \tag{17.A1}$$

where V_δ is the so-called exclusion volume which is used to remove the singularity of $\widetilde{G}^{NF}$ at $\mathbf{R} = \mathbf{R}'$ and $\widetilde{L}$ is the source dyadic accounting depolarizing properties of V_δ, which depends solely on the shape of the exclusion volume [36, 37].

Choosing the origin of a Cartesian coordinate system on the surface of the plasmonic film with the z-axis directed along the axis of the cylindrical particle, as shown in Fig. 17.2, for our case $\widetilde{L}$ has the next simple diagonal form:

$$\widetilde{L} = 0.5a(\xi)\widetilde{U}_t + (1-a(\xi))\left(e_z \bigotimes e_z\right), \tag{17.A2}$$

where $a(\xi) = 1/\sqrt{1+\xi^2}$ and $\xi = d/h_p$ with $\widetilde{U}_t = \left(e_i \bigotimes e_i\right)$ the transversal unit tensor $\mathbf{e}_i$ $(i = x, y)$ and $\mathbf{e}_z$ denote unit vectors in a Cartesian xyz-coordinate system.

According to the method developed in [26], we suppose that similar to Eq. (17.2) for the local current density $\mathbf{j}(\mathbf{R},\omega)$, one can introduce the relation connecting $\mathbf{j}(\mathbf{R},\omega)$ with the external field $\mathbf{E}^{(0)}(\mathbf{R},\omega)$ illuminating the system:

$$j(R,\omega) = -i\omega\varepsilon_0\widetilde{\chi}^{(S)}(R,\omega)E^{(0)}(R,\omega), \tag{17.A3}$$

where $\widetilde{\chi}^{(S)}(R,\omega)$ is the tensor of linear response of the particle on the surface to the external field $\mathbf{E}^{(0)}(\mathbf{R},\omega)$. Then using the constitutive relation Eq. (17.2) in the form

$$j(R,\omega) = -i\omega\varepsilon_0\widetilde{\chi}(\omega)E(R,\omega), \tag{17.A4}$$

and Eq. (17.A3), the external field can be expressed as

$$E^{(0)}(R,\omega) = \left(\widetilde{\chi}^{(S)}(R,\omega)\right)^{-1}\widetilde{\chi}(\omega)E(R,\omega). \tag{17.A5}$$

The reverse matrix $\left(\widetilde{\chi}^{(S)}(R,\omega)\right)^{-1}$ exists because there is dissipation in the system.

Substituting Eq. (17.A4) into Eq. (17.A1), one obtains analogously to [26]

$$\begin{aligned} E(R,\omega) = {} & \left(\widetilde{\chi}^{(S)}(R,\omega)\right)^{-1}\widetilde{\chi}(\omega)E(R,\omega) \\ & -k_0^2 \lim_{\delta\to 0}\int\limits_{V-V_\delta} dR'\widetilde{G}^{NF}\left(R,R',\omega\right)\widetilde{\chi}(\omega)E\left(R',\omega\right) + \widetilde{L}\widetilde{\chi}(\omega)E(R,\omega). \end{aligned} \tag{17.A6}$$

Since Eq. (17.A6) fulfills for all points of the system including points within the volume V - V_δ, we can act on Eq. (17.A6) by the operator $\lim\limits_{\delta\to 0}\int\limits_{V-V_\delta} dR$. Then, supposing that local field can be represented in the form [26]

$$E(R,\omega) = \sum_K E(K,\omega)\exp(i\mathrm{KR}), \tag{17.A7}$$

after interchanging of the dummy variables $R' \leftrightarrow R$ and, correspondingly, the order of integration, one obtains from Eq. (17.A6)

$$\begin{aligned} \sum_K \lim_{\delta\to 0}\int\limits_{V-V\delta} dR\Bigg\{ & \widetilde{U} - \widetilde{L}\widetilde{\chi}(\omega) + k_0^2 \lim_{\delta\to\infty}\int\limits_{V-V_\delta} dR'\widetilde{G}^{NF}\left(R',R,\omega\right)\widetilde{\chi}(\omega) \\ & - \left(\widetilde{\chi}^{(S)}(R,\omega)\right)^{-1}\widetilde{\chi}(\omega)\Bigg\}E(K,\omega)\exp(i\mathrm{KR}) = 0. \end{aligned} \tag{17.A8}$$

Using the fact that exponents form the complete set of orthonormal functions, we obtain from Eq. (17.A8)

$$\widetilde{\chi}^{(S)}(R,\omega) = \widetilde{\chi}(\omega)\left[\widetilde{U} + \left(k_0^2 \lim_{\delta\to 0}\int\limits_{V-V_\delta} dR'\widetilde{G}^{NF}\left(R',R,\omega\right) - \widetilde{L}\right)\widetilde{\chi}(\omega)\right]^{-1}. \tag{17.A9}$$

Using Eqs. (17.A3), (17.A4), and (17.A9), one can receive the relation between the local and external fields existing within the volume $V - V_\delta$:

$$E(R,\omega) = \widetilde{\Theta}(R,\omega)E^{(0)}(R,\omega), \tag{17.A10}$$

$$\widetilde{\Theta}(R,\omega) = \left[\widetilde{U} + \left(k_0^2 \lim_{\delta\to 0} \int\limits_{V-V_\delta} dR' \widetilde{G}^{NF}(R',R,\omega) - \widetilde{L}\right)\widetilde{\chi}(\omega)\right]^{-1}. \tag{17.A11}$$

The electric dipole moment of the current density distribution $\mathbf{j}(\mathbf{R},\omega)$

$$p(\omega) = (i/\omega)\int\limits_V d\mathrm{Rj}(R,\omega). \tag{17.A10}$$

Taking into account Eq. (17.A4), it can be rewritten in the form

$$p(\omega) = \varepsilon_0\widetilde{\chi}(\omega)\int\limits_V d\mathrm{RE}(R,\omega). \tag{17.A11}$$

Replacing the local field $\mathbf{E}(\mathbf{R},\omega)$ in Eq. (17.A11) by the external field $\mathbf{E}^{(0)}(\mathbf{R},\omega)$, we obtain

$$p(\omega) = \varepsilon_0\widetilde{\chi}(\omega)\int\limits_V dR\widetilde{\Theta}(R,\omega)E^{(0)}(R,\omega). \tag{17.A12}$$

Since we consider nanoparticles with sizes less than the wavelength of the external illuminating field, one can omit the variation of the external field across the particle, i.e., in Eq. (17.A12), one can replace $\mathbf{E}^{(0)}(\mathbf{R},\omega)$ by $\mathbf{E}^{(0)}(\mathbf{R}_\mathrm{c},\omega)$, then

$$p(\omega) = \varepsilon_0\widetilde{\chi}(\omega)\left[\int\limits_V dR\widetilde{\Theta}(R,\omega)\right]E^{(0)}(R_c,\omega), R_c = (\mathbf{0},z_c). \tag{17.A13}$$

Evaluating the integral in square brackets of Eq. (17.A13) as

$$\left[\int\limits_V dR\widetilde{\Theta}(R,\omega)\right] \approx V\widetilde{\Theta}(R_c,\omega) \tag{17.A14}$$

we can introduce the dyadic dipole-dipole polarizability of the particle via

$$\widetilde{\alpha}(\omega) = \varepsilon_0 V\widetilde{\chi}^{(S)}(\omega). \tag{17.A15}$$

The tensor $\widetilde{\chi}^{(S)}(\omega)$ for the considered case has the diagonal form

$$\widetilde{\chi}^{(S)}(\omega) = \chi_{\parallel}^{(S)}(\omega)U_t + \chi_{\perp}^{(S)}(\omega)\left(e_z \bigotimes e_z\right) \quad (i = x, y) \tag{17.A16}$$

with the components of the polarizability written as

$$\chi_q^{(S)}(\omega) = \chi(\omega)/\left(1 + A_q(\omega;\xi)\right) \ (q = \parallel, \perp), \tag{17.A17}$$

where

$$A_{\parallel}(\omega;\xi) = 0,25(-1 + a(\xi)(3 + 0,5\eta(\omega)) - 1,5b(\xi)\eta(\omega)), \tag{17.A18}$$

$$\begin{aligned} A_{\perp}(\omega;\xi) = {} & -0,5 \\ & + 0,25\left(-a(\xi)\left(6 - \eta(\omega)\left[3 + 4/\xi^2\right]\right) + b(\xi)\eta(\omega)\left[1 + 12/\xi^2\right]\right), \end{aligned} \tag{17.A19}$$

$$b(\xi) = 1/\sqrt{9 + \xi^2}, \eta(\omega) = (\varepsilon_2(\omega) - \varepsilon_3)/(\varepsilon_2(\omega) + \varepsilon_3), \tag{17.A20}$$

ε_3 is a dielectric function of surrounding medium.

Calculation of the Susceptibility of a Nanoparticle Layer

Let us suppose that the tensor of linear response of the cylindrical particle on the surface of an active medium $\widetilde{\chi}^{(S)}(\omega)$ is known; then the electric field in the medium "3" where the particles are located can be written in the form similar to Eq. (17.5):

$$E^{(3)}(k, z, \omega) = E^{(03)}(k, z, \omega) - \rho\widetilde{G}^{(33)}(k, z, z_c, \omega)\widetilde{\chi}^{(S)}(\omega)E^{(3)}(k, z_c, \omega), \tag{17.B1}$$

where $E^{(03)}(k, z, \omega)$ is the external long-range electrical field acting on the particle in the layer

$$E^{(03)}(k, z, \omega) = -i\mu_0\omega \int_{l_0} dz'' \widetilde{G}^{(31)}(k, z, z'', \omega) j^{1ext}(k, z'', \omega). \tag{17.B2}$$

Let us assume that the Green function of the considered system $\widetilde{F}^{(31)}$ is known, then

$$E^{(3)}(k, z, \omega) = -i\mu_0\omega \int_{l_0} dz'' \widetilde{F}^{(31)}(k, z, z'', \omega) j^{1ext}(k, z'', \omega). \tag{17.B3}$$

Substituting Eq. (17.B3) into Eq. (17.B1), one can write

$$\widetilde{F}^{(31)}(k,z,z'',\omega)+\rho\widetilde{G}^{(33)}(k,z,z_c,\omega)\widetilde{\chi}^{(S)}(\omega)\widetilde{F}^{(31)}(k,z_c,z'',\omega) -\widetilde{G}^{(03)}(k,z,z'',\omega)=0. \tag{17.B4}$$

Taking Eq. (17.B4) at the point $z=z_c$ and using Eq. (17.B3), we obtain the simple relation between the local field $\mathbf{E}^{(3)}$ and the external field $\mathbf{E}^{(03)}$ at the point $z=z_c$:

$$E^{(3)}(k,z_c,\omega)=\widetilde{\Omega}(k,z_c,z_c,\omega)E^{(03)}(k,z_c,\omega), \tag{17.B5}$$

$$\widetilde{\Omega}(k,z_c,z_c,\omega)=\left[\widetilde{U}+\rho\widetilde{G}^{(33)}(k,z_c,z_c,\omega)\widetilde{\chi}^{(S)}(\omega)\right]^{-1}. \tag{17.B6}$$

The tensor $\widetilde{\Omega}(k,z_c,z_c,\omega)$ is the dimensionless effective susceptibility of the layer of cylindrical nanoparticles on a surface [16, 17], which accounts both near- and far-field electromagnetic interactions within the layer and with the substrate.

References

1. Agranovich VM, Mills DL (eds) (1982) Surface polaritons: electromagnetic waves at surfaces and interfaces. North Holland, Amsterdam
2. Raether H (1988) Surface plasmons on smooth and rough surfaces and on gratings. Springer, Berlin. https://doi.org/10.1007/BFb0048317
3. Franzen S (2008) Surface plasmon polaritons and screened plasma absorption in indium tin oxide compared to silver and gold. J Phys Chem C 112(15):6027–6032. https://doi.org/10.1021/jp7097813
4. Harrick NJ (1967) Internal reflection spectroscopy. Wiley, New-York
5. Kretschmann E, Raether H (1968) Radiative decay of non-radiative surface plasmons excited by of non-radiative surface plasmons excited by light. Z Naturforsch A23:2135–2136. https://doi.org/10.1515/zna-1968-1247
6. Homola J, Yee SS, Gauglitz G (1999) Surface plasmon resonance sensors: review. J Sensors Actuators B: Chem 54(1–2):3–15. https://doi.org/10.1016/S0925-4005(98)00321-9
7. Gwon HR, Lee SH (2010) Spectral and angular responses of surface Plasmon resonance based on the Kretschmann prism configuration. Mater Trans 51(6):1150–1155. https://doi.org/10.2320/matertrans.M2010003
8. Devanarayanan VP, Manjuladevi V, Gupta RK (2016) Surface plasmon resonance sensor based on a new opto-mechanical scanning mechanism. Sensors Actuators B: Chem 227:643–648. https://doi.org/10.1016/j.snb.2016.01.027
9. Ilchenko SG, Lymarenko RA, Taranenko VB (2017) Using metal-multilayer-dielectric structure to increase sensitivity of surface Plasmon resonance sensor. Nanoscale Res Lett 12:295. https://doi.org/10.1186/s11671-017-2073-1
10. Boardman AD (1982) Electromagnetic surface modes. Wiley, New York
11. Kreibig U, Vollmer M (1995) Optical properties of metal clusters. Springer, Berlin. https://doi.org/10.1007/978-3-662-09109-8
12. Lance KL, Coronado E, Zhao LL, Schatz GC (2003) The optical properties of metal nanoparticles: the influence of size, shape, and dielectric environment. J Phys Chem B 107 (3):668–677. https://doi.org/10.1021/jp026731y
13. Hutter E, Fendler JH (2004) Exploitation of localized surface plasmon resonance. Adv Mater 16 (19):1685–1706. https://doi.org/10.1002/adma.200400271

14. Chegel V, Demidenko Y, Lozovski V, Tsykhonya A (2008) Influence of the shape of the particles covering the metal surface on dispersion relations of surface plasmons. Surf Sci 602 (8):1540–1546. https://doi.org/10.1016/j.susc.2008.02.015
15. Chen W-Y, Lin C-H (2010) A standing-wave interpretation of plasmon resonance excitation in split-ring resonators. Opt Express 18(13):14280–14292. https://doi.org/10.1364/OE.18.014280
16. Baryakhtar I, Demidenko Y, Lozovski V (2013) Interaction between localized-on-nanoparticles plasmon polaritons and surface plasmon polaritons. J Opt Soc Am B 30(4):10200–11026. https://doi.org/10.1364/JOSAB.30.001022
17. Demydenko Y, Juodkazis S, Lozovski V (2014) Composite Au-on-SiC nanorods for sensing. J Opt Soc Am B 31(11):2893–2900. https://doi.org/10.1364/JOSAB.31.002893
18. Malynych S, Chumanov G (2003) Light-induced coherent interactions between silver nanoparticles in two-dimensional arrays. J Am Chem Soc 125(10):2896–2898. https://doi.org/10.1021/ja029453p
19. Balci S, Karademir E, Kocabas C (2015) Strong coupling between localized and propagating plasmon polaritons. Opt Lett 40(13):3177–3180. https://doi.org/10.1364/OL.40.003177
20. Guo L, Jackman JA, Yang H–H, Chen P, Cho N–J, Kim D–H (2015) Strategies for enhancing the sensitivity of plasmonic nanosensors. J Nanotoday 10(2):213–239. https://doi.org/10.1016/j.nantod.2015.02.007
21. Stewart ME, Anderton CR, Thompson LB, Maria J, Gray SK, Rogers JA, Nuzzo RG (2008) Nanostructured plasmonic sensors. Chem Rev 108(2):494–521. https://doi.org/10.1021/cr068126n
22. Li M, Cushing SK, Wu N (2015) Plasmon-enhanced optical sensors: a review. Analyst 140 (2):386–406. https://doi.org/10.1039/C4AN01079E
23. Khudik, B.I., Lozovskii, V.Z., and Baryakhtar, I.V.: Macroscopic electrodynamics of ultra-thin films. Phys Status Solidi B 153(1), 167–177 (1989). doi: https://doi.org/10.1002/pssb.2221530117
24. Keller O (1996) Local fields in electrodynamics of mesoscopic media. Phys Rep 268:85–262. https://doi.org/10.1016/0370-1573(95)00059-3
25. Demidenko Y, Makarov D, Krone P, Lozovski V (2009) Effect of a magnetic field on the optical properties of nonmagnetic nanorods in a dielectric matrix. J Opt A Pure Appl Opt 11 (12):125001. https://doi.org/10.1088/1464-4258/11/12/125001
26. Lozovski V (2010) The effective susceptibility concept in the electrodynamics of nano-system. J comput Theor Nanosci 7(7):1–17. https://doi.org/10.1166/jctn.2010.1588
27. Demidenko YV, Makarov D, Lozovski V (2010) Local-field effects in magneto-plasmonic nanocomposites. J Opt Soc Am B 27(12):2700–2706. https://doi.org/10.1364/JOSAB.27.002700
28. Haarmans MT, Bedeaux D (1993) The polarizability and the optical properties of lattices and random distributions of small metal spheres on a substrate. Thin Solid Films 224(1):117–131. https://doi.org/10.1016/0040-6090(93)90468-5
29. Bah ML, Akjouj A, Dobrzynski L (1992) Response functions in layered dielectric media. Surf Sci Rep 16(3):97–131. https://doi.org/10.1016/0167-5729(92)90010-9
30. Kolwas K, Derkachova A (2013) Damping rates of surface plasmons for particles of size nano- to micrometers; reduction of the nonradiative decay. JQSRT 114:45–55. https://doi.org/10.1016/j.jqsrt.2012.08.007
31. von Rottkay, K., Rubin, M.: Optical indices of pyrolytic tin-oxide glass. Mater Res Soc Symp Proc 426, 449–456 (1996). doi: https://doi.org/10.1557/PROC-426-449
32. Persson BNJ (1983) Lateral interactions in small particle systems. J de Physique 44(C10) C10-409-C10-419. https://doi.org/10.1051/jphyscol:19831084
33. Törmä P, Barnes WL (2015) Strong coupling between surface plasmon polaritons and emitters: a review. Rep Prog Phys 78**,** 013901-1-34. https://doi.org/10.1088/0034-4885/78/1/013901
34. Abrickosov AA, Gor'kov LP, Dzyaloshinskii IY (1965) Quantum field theoretical methods in statistical physics. Pergamon, Oxford

35. Lifshitz EM, Pitaevskii LP (1980) Statistical physics (Part.2), course of theoretical physics, vol 9. Pergamon, Oxford
36. Yaghjian AD (1980) Electric dyadic green's functions in the source region. Proc IEEE 68 (2):248–263. https://doi.org/10.1109/PROC.1980.11620
37. van Bladel, J.: Singular electromagnetic fields and sources. Clarendon, Oxford (1991). doi: https://doi.org/10.1137/1034110